

# Influence of transmutation-induced Re/Os content on defect evolution in neutron-irradiated W

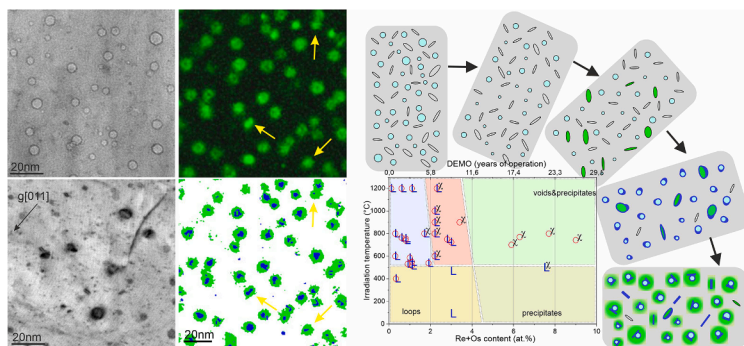
M. Klimenkov<sup>a,\*</sup>, U. Jäntsch<sup>a</sup>, M. Rieth<sup>a</sup>, H.C. Schneider<sup>b</sup>, D. Terentyev<sup>c</sup>, W. Van Renterghem<sup>c</sup>

<sup>a</sup> Karlsruhe Institute of Technology (KIT), Institute for Applied Materials- Applied Materials Physics, Karlsruhe, 76021, Germany

<sup>b</sup> Karlsruhe Institute of Technology (KIT), Institute for Applied Materials - Mechanics of Materials and Interfaces, Karlsruhe, 76021, Germany

<sup>c</sup> SCK CEN, Nuclear Materials Science Institute, Boeretang 200, Mol, 2400, Belgium

## GRAPHICAL ABSTRACT



## ARTICLE INFO

### Keywords:

Tungsten  
Neutron irradiation  
Microstructure  
Transmutation  
Voids  
Radiation induced defects

## ABSTRACT

The microstructure of neutron irradiated tungsten (0.1 dpa - 0.8 dpa at  $T_{irr} = 1200$  °C), was analyzed by transmission electron microscopy applying high-sensitivity energy dispersive X-ray spectroscopy, which enables the visualization of the distribution of transmutation induced Re and Os. The study demonstrates the dose-dependent evolution of radiation-induced defects such as voids and dislocation loops as well as segregation behavior of Re and Os at these defects. Re segregation around voids occurs at the lowest damage dose of 0.1 dpa, while their enrichment on dislocation loops was detected at 0.2 dpa. Further generation of Re and Os leads to the formation of the  $\chi$ -phase  $((Re,Os)_3W)$  precipitates with a needle shape on voids and on dislocation loops. The formation of Os-rich nuclei within Re clouds around loops or voids is crucial for the onset of precipitate formation. It could be shown that the subsequent formation of precipitates on dislocation loops causes the disappearance of the loops. Based on these results, a modification of a well-known defect formation diagram in W has been proposed as a function of the Re/Os content. This would provide a comparison of defect evolution in W irradiated in reactors with different transmutation rates. It would also allow a prediction of the microstructural evolution in W under fusion conditions.

\* Corresponding author.

E-mail address: [michael.klimenkov@kit.edu](mailto:michael.klimenkov@kit.edu) (M. Klimenkov).

<https://doi.org/10.1016/j.jnucmat.2024.154950>

Received 10 October 2023; Received in revised form 24 January 2024; Accepted 3 February 2024

Available online 5 February 2024

0022-3115/© 2024 The Authors. Published by Elsevier B.V. This is an open access article under the CC BY license (<http://creativecommons.org/licenses/by/4.0/>).

## 1. Introduction

Due to its favorable properties, such as a very high melting point in combination with high creep and sputter resistance, W is considered as the most promising material for high-temperature vacuum or inert gas applications in energy technology. In particular, the W plasma-facing structural parts of fusion reactors must be able to operate at very high temperatures and withstand a significant degree of radiation-induced damage [1–3]. This challenge requires a detailed knowledge of the degradation of the mechanical properties under irradiation and the formation of irradiation induced defects. A detailed experimental understanding of neutron damage processes at the nanoscale, which is currently limited, is of utmost importance for material qualification. Knowledge of the process of defect formation and evolution in neutron irradiated tungsten (W) is essential not only for assessing its suitability (or applicability) as a structural material in fusion reactors, but also for understanding numerous irradiation experiments in fission reactors.

Extensive microstructural characterizations of W have already been carried out to understand its microstructural response to neutron irradiation [3–12]. The numerous publications show that in W three types of radiation defects are formed: voids, dislocation loops and precipitates. The studies however are often "snapshot" microstructures that form under certain ( $T_{\text{irr}}$ , damage dose, content of transmutation induced Re and Os, etc.) conditions. Conclusions regarding the evolution of the microstructure with increasing damage are then only possible by comparison of the experimental data obtained from different irradiation experiments and thus at different irradiation temperature, different uncertainty in the determination of the irradiation temperature and different reactors with different transmutation rates. However, these varying conditions significantly limit the validity of such conclusions. Obviously, there is a lack of studies investigating dose-dependent defect formation in W irradiated under the same conditions ( $T_{\text{irr}}$  and reactor), which would allow an investigation of defect evolution with increasing damage doses. In the presented work we show detailed investigation of voids and dislocation loops in W irradiated at 1200 °C to a 0.1 dpa, 0.2 dpa, 0.5 dpa and 0.8 dpa damage dose. It could be demonstrated that Re and Os segregation takes place at the lowest doses. Consideration of their evolution could provide the decisive influence of transmutation products on the development of defects in neutron-irradiated W. We also propose the defect formation sequence that demonstrate Re and Os segregation on different irradiation stages as well its influence on the evolution of loops and voids.

The diagram that reflects the formation of defects depending on the temperature and damage dose was proposed by Hasegawa et al. [4] and later modified by Marian et al. [13] and Koyanagi et al. [8]. This diagram was also extended with the new data in recent review article by Hu [14]. The diagrams illustrate the irradiation conditions for the formation of different types of dislocations and their evolution with increasing damage dose. The diagrams show a disappearance of dislocation loops as the damage and consequently the transmutation-induced Re and Os content increases [13,14]. This process was followed by increased formation of precipitates, that become dominant defect type at higher damage doses. It should be mentioned that these diagrams were made based on the results of TEM imaging, where precipitates have typical acicular shape and crystalline structure. Consequently, the precipitates are well visible in TEM images based on diffraction contrast. However, several publications show that Re and Os-rich clouds have been formed around voids and dislocation loops, but these "clouds" do not show any contrast in TEM images. Their presence could only be detected by energy dispersive X-ray analysis (EDX) or atomic probe tomography (APT) [5,6,8,10,15]. Based on the results obtained in the framework of this work, we propose that the defect formation diagram should show dependence on the Re/O content in the final state and not on the damage doses.

The comparison of W irradiated in different reactors shows significant differences in the outcome despite the very similar irradiation conditions [4]. It is obvious that the formation and development of

defects depends not only on the neutron flux and temperature, but also on the specific neutron spectrum that determines the transmutation rates of the different isotopes. Therefore, the reactor type, the design of the testing rigs, and the exact irradiation position within the reactor are highly relevant for the interpretation of the experimental results. As a consequence, the outcome of an irradiation campaign has to be considered as a unique result, which adds to a more complete systematization, understanding and thereby prediction of neutron radiation damage. The proposed modification would allow comparison of the results achieved in irradiation experiments in different reactors with different transmutation rates.

## 2. Experimental

The investigated polycrystalline W with a purity of 99.97 wt.% was provided by PLANSEE SE, Austria. The material was cold rolled to a high degree of deformation into a 1 mm thick plate. The material is subsequently annealed to relieve the mechanical stresses. The samples were irradiated by neutrons to damage doses between about 0.1 and 0.8 dpa at 1200 °C in the Belgian Nuclear Research Center SCK-CEN, Mol (Belgium) (see Table 1 for exact irradiation doses and content of transmutation products). The irradiation was performed directly inside a channel within a fuel element. The irradiation rig was made of a tick-wall pressurized tube, which had a dual function: pressure-barrier and shielding to screen thermal neutrons. The irradiation was performed in Helium to prevent oxidation under high temperature irradiation exposure. The gas pressure and the gap between the samples and the capsule wall were designed according to thermal and neutronics calculations in order to achieve the target irradiation temperature. Hence, the temperature was achieved through the balance of the irradiation-induced heat release inside the specimens and holders (gamma heating), and the heat evacuation through the gas gap to the capsule wall and the reactor cooling water. The in-situ temperature of the specimens could not be controlled or monitored in this irradiation experiment, since the capsules were leak-tight sealed by welding precluding instrumentation. Four irradiation doses were thus realized in four irradiation capsules. The capsules were placed in the mid-plane position (positions corresponding to the most stable flux during the cycle) inside of four different irradiation channels. The irradiation up to 0.124 dpa took one cycle (28 days), 0.183 – two cycles, 0.507 – 4 cycles, and 0.819 – 6 cycles. The former experience with the same design of the irradiation capsules and application of SiC post-irradiation thermometry suggests that the target irradiation temperature could be achieved with an accuracy of about 10 % of the absolute temperature.

The total irradiation time was 28–186 days (depending on the specific capsule) and the neutron flux was  $(1.5\text{--}2.6) \times 10^{14}$  ( $E > 0.1$  MeV),  $(0.6\text{--}1.2) \times 10^{14}$  ( $E > 1$  MeV) n/cm<sup>2</sup>/s. The neutron flux was calculated using the MCNPX 2.7.0 code as well as confirmed by dosimetry measurements using Fe and Nb dosimeters, applied to measure the fast neutron fluence ( $> 1$  MeV) [16]. The dpa cross sections for W have been prepared from the JENDL4 file (MT444) for a threshold displacement energy of 55 eV.

Since the material is radioactive, it was advantageous to use a focused ion beam milling (FIB) for sample preparation in order to (i) limit the activity of the TEM samples, which interferes with the chemical analysis and (ii) perform sample preparation in a pre-defined area. The thin lamellae were prepared in a Scios FIB/SEM instrument (product of Thermo Fisher Scientific Inc.) and attached to a molybdenum grid. After preparation and initial examination including study of void distribution,

**Table 1**

Content of transmutation induced elements for different damage doses.

damage dose (dpa)	0.124	0.183	0.507	0.819
Re (FISPACT) (at.%)	0.423	0.592	1.74	2.15
Os (FISPACT) (at.%)	0.008	0.0153	0.149	0.239

the lamellae were flash polished in 1 % NaOH water solution using the method described in the Ref. [17] to remove defects introduced during ion beam milling. This step facilitates the analysis of dislocation loops, which are poorly visible due to the surface damage caused by the FIB.

The microstructural examination was carried out using a Talos F200X transmission electron microscope (TEM) (product of Thermo Fisher Scientific Inc.) equipped with four energy-dispersive X-ray (EDX) detectors. The EDX detector resolution is specified by the manufacturer as  $\leq 136$  eV at Mn-K $_{\alpha}$ . At the W-L $_{\alpha}$  ( $E = 8.396$  keV) the energy resolution has a value of about 150–160 eV, which is sufficient to separate the W-L $_{\alpha}$ , Re-L $_{\alpha}$  and Os-L $_{\alpha}$  X-ray lines. The TEM images and selected area diffraction pattern (SAED) were acquired by using a Ceta 16 M CCD camera. The STEM-EDX maps were acquired in the Velox software using  $512 \times 512$  pixels and a spectral dispersion of 5 eV. ImageJ soft was used for statistical analysis of TEM images [18].

Voids were visualized using bright field (BF) imaging in under-focus, displaying them with bright contrast compared to the matrix. The images of loops were taken using diffraction contrast in the dark field (DF) imaging applying scanning TEM (STEM) [19]. Loops were analysed within grains oriented with  $\langle 110 \rangle$  g-vectors near the [100] zone axis. The thickness of the sample that was used for number density calculations was measured using low loss electron energy loss spectroscopy (EELS). Due to the considerable local thickness variations caused by flash polishing, the average thickness of the examined area was used to calculate the defect density.

### 3. Result

The study includes a detailed TEM characterization of the radiation-induced defects, which can be divided into three types, e.g. voids, dislocation loops and precipitates. In addition, a dose-dependent segregation of Re and Os, i.e. the formation of "clouds" around defects, was observed. In this work, we use the terms "precipitation" or "precipitates" to refer to the formation of second-phase precipitates, e.g.,  $\chi$ -phase in this case. The precipitates could be detected either by high resolution TEM or by EDX elemental mapping, where they are visible in elongated shape. The term "segregation" has been used to refer to the

process of Re and Os enrichment around structural defects, while the term "cloud" is used to denote areas around defects enriched by Re and/or Os. The "clouds" exhibit a bcc structure of pure W and are visible only in high sensitive elemental maps. As the study is concerned with the early stages of defect formation, the distinctions between Re/Os-rich clouds and  $\chi$ -phase precipitates are not always clear.

#### 3.1. Distribution of voids, loops and precipitates

Fig. 1 shows the void and dislocation loops microstructure formed in W irradiated at four different damage doses. The images of voids (Fig. 1a-d) were taken using BF mode, whereas DF mode was applied for visualization the dislocation loops (Fig. 1a'-d'). The voids are mostly round or almost round in shape, but in a few cases faceted voids with a size of 3–4 nm have been observed, similar to that reported in Ref. [6]. The morphology of the voids does not change significantly with increasing damage dose, indicating that their main formation occurs at doses below 0.1 dpa.

Dislocation loops are typically visible in DF images with a "coffee bean" contrast (Fig. 1a'-d'). Most loops are between 3 and 10 nm, but individual loops can be up to 20 nm. The number density of dislocation loops at 0.1 dpa and 0.2 dpa is comparable to the number density of voids, while for material irradiated to 0.5 dpa and higher, the number density is reduced by about two orders of magnitude. This reduction in number density is related to the segregation of Re and Os and the growth of  $\chi$ -phase precipitates.

The contents of transmutation induced Re and Os calculated for the different damage doses are shown in the Table 1. Their spatial distribution was studied by STEM-EDX element mapping in the TEM, where the local presence was visualized by intensity variations of the different colors. Fig. 2 demonstrates the distribution of Re (green) and Os (blue) in representative areas in the material irradiated at all damage doses. All maps were acquired at the same magnification. At 0.1 dpa and 0.2 dpa, the Re distribution was detected only around the voids, while the Re signal at the dislocation loops was seemingly below the detection limit. There was no Os signal detected in 0.1 dpa damage, while a weak Os signal was detectable in the material with 0.2 dpa. At 0.5 dpa and 0.8

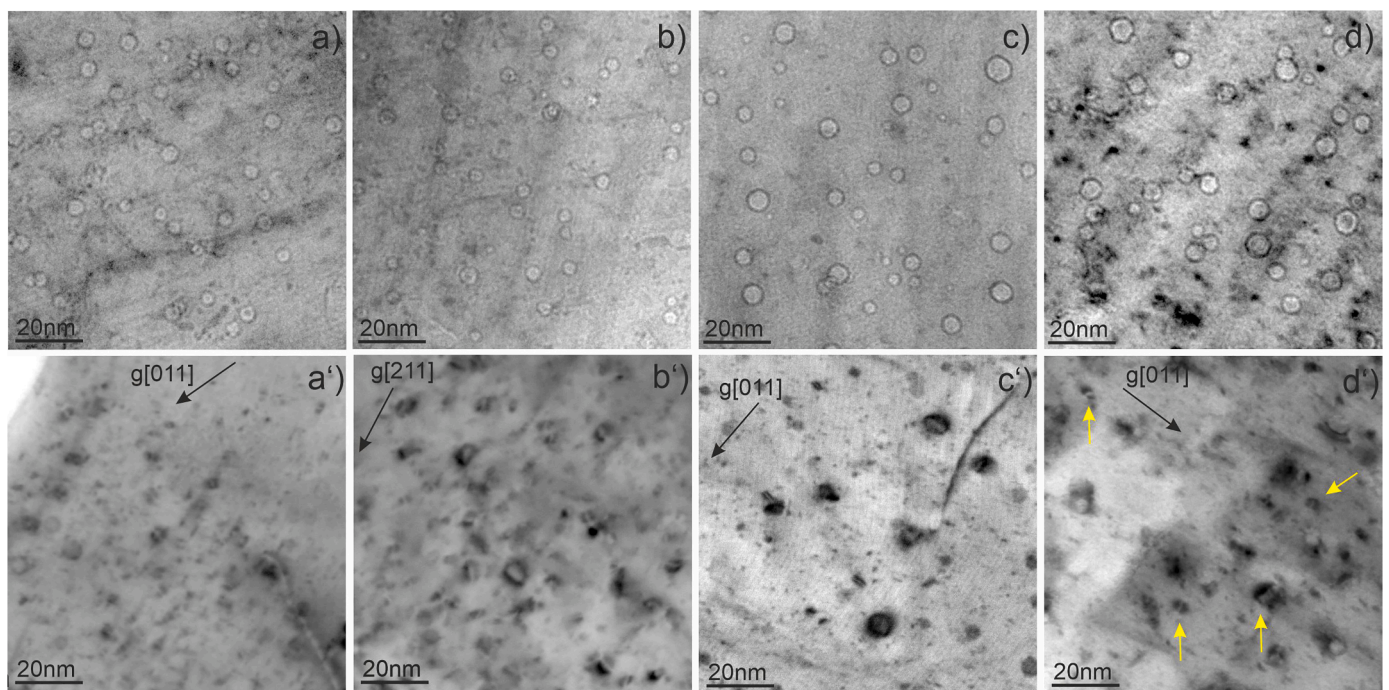
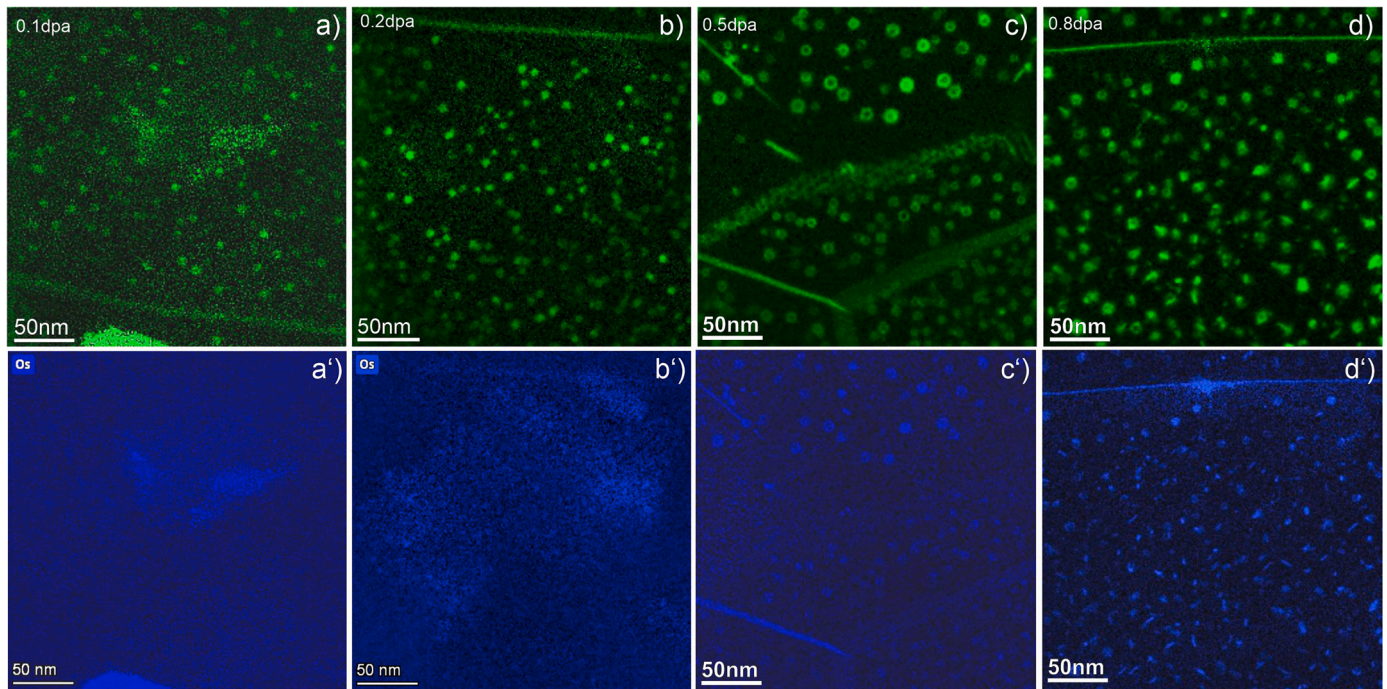


Fig. 1. BF-TEM images showing voids in W irradiated to 0.1 dpa (a), 0.2 dpa (b), 0.5 dpa (c) and 0.8 dpa (d). The second row (images from a' to d') show the DF-TEM images of dislocation loops with inverted contrast .



**Fig. 2.** *Re* (green) and *Os* (blue) EDX maps showing the segregation on grain boundaries, voids and dislocation loops in W irradiated to 0.1 dpa (a,a'), 0.2 dpa (b,b'), 0.5 dpa (c,c') and 0.8 dpa (d,d').

dpa, *Re* was detected around voids and loops. At 0.5 and 0.8 dpa, the occurrence of *Os* is clearly detectable and was found in the areas of *Re*-segregation. *Re*- and *Os*-segregation at the grain boundaries was observed at all damage doses. In the case of sub grain boundaries, *Re*-segregation is clearly seen at the grain boundary dislocations (Fig. 2c). Nanoscale *Re*- and *Os*-rich precipitates next to the voids and on with mostly elongated shape were evident at 0.8 dpa and in very small numbers at 0.5 dpa.

The statistical data of radiation induced defects are shown in Fig. 3, indicating the size (a) and the number density (a) of defects. The size of the voids increases slightly from 3.2 nm to 4.3 nm whereas the number density slightly decreases from  $8 \times 10^{22} \text{ m}^{-3}$  to  $5 \times 10^{22} \text{ m}^{-3}$ , as the damage dose increases from 0.1 dpa to 0.8 dpa. The size of the dislocation loops, on the other hand, shows a maximum at 0.5 dpa. The number density of the loops shows a similar value as for the voids at 0.1 dpa and 0.2 dpa damage and reduces a factor 10 at 0.5 dpa and factor 30 at 0.5 dpa (Fig. 3b). The nanometer sized precipitates were observed in the very low amount at 0.5 dpa, whereas at higher damage dose (0.8 dpa) their number increased rapidly by a factor of 50. The average size of precipitates increases here from 3 nm at 0.5 dpa to 4.5 nm at 0.8 dpa.

### 3.2. Detailed analysis of *Re* and *Os* segregation on radiation induced defects

The results presented in this section should illustrate the development of the *Re* and *Os* segregation process on voids and dislocation loops and determine the formation of precipitates at higher damage doses. The results must explain the reasons for the disappearance of dislocation loops, as suggested by Marian et al. [13]. To this purpose, we have performed a detailed, high-sensitivity EDX element mapping that can visualize even the smallest *Re*- and *Os* segregations at different damage doses.

Fig. 4 shows that at a damage dose of 0.2 dpa, segregation of *Re* was detected only around voids and only in few cases around loops. The voids visible in the BF image (a) and the same positions in the *Re* map (c) are marked with circles. A good correlation suggests that all voids are surrounded by a *Re*-rich "cloud". The largest loops marked by squares in

the DF image (b) and in the *Re* map (c) show no detectable *Re* content. *Re* was detected only on one dislocation loop marked by a yellow square. Probably, segregation of transmutation products takes place, but the concentration is lower than the detection limit of the EDX system used.

A clear *Re* and *Os* segregation around voids and dislocation loops was detected at 0.5 dpa, when their cumulative content increases to 1.9 %. In the Fig. 5 the three loops visible in DF image loops (a) are numbered and marked in *Re* (b), *Os* (c) maps and in the overlap image (d). The corresponding intensity profiles are shown in the images (e<sub>1</sub>), (e<sub>2</sub>), and (e<sub>3</sub>). The loops (1) show a well detectable *Re*-rich cloud of 9 nm size, however no *Os* segregation was detected (profile in e<sub>1</sub>). The loops (2) and (3) show 7 nm and 9 nm *Re* clouds and additionally well detectable *Os* rich segregation of elongated shape (profiles in e<sub>2</sub> and e<sub>3</sub>). The thickness of the *Os*-rich core is about 2–3 nm (d). This observation is consistent with the finding that *Os* preferentially segregates at the dislocation line of a loop, while *Re* surrounds a defect [10]. In this case, the imaged dislocation loops have an "on-edge" (or slightly tilted) orientation to the imaging plane. In this orientation, a loop and *Os* attached on dislocation line the would be visible as a narrow strip. The nanosized precipitates of the  $\chi$ -phase seen in ref. [10] would have the same (or very similar) *Re* and *Os* distribution. However, numerous HRTEM imaging of a region with dislocation loops give no indication of the formation of *Re*- or *Os*-rich precipitates with a defined crystalline structure.

The detailed analysis of *Re* and *Os* segregation on defects in the sample irradiated to 0.8 dpa is shown in Fig. 6. The distribution of *Re* (green) and *Os* (blue) are visualize in corresponding elemental maps (b and c) and shown overlapped in the part (d). The overlapping clearly show that *Os* tends to form small rich areas inside *Re* clouds which mostly have a spherical shape. *Os*-rich areas often have a needle-like shape, indicating the formation of precipitates or their precursor. These *Os*-rich areas are formed on both voids and dislocation loops. The void marked with arrow (1) has for example two acicular precipitates that form an angle of  $\sim 45^\circ$  to each other. At this damage often was also observed that some spherical *Re* rich clouds have been formed on the locations without a void – suggesting the formation of precipitates on the loops.

To visualize the *Os* distribution more clearly the intensity profile

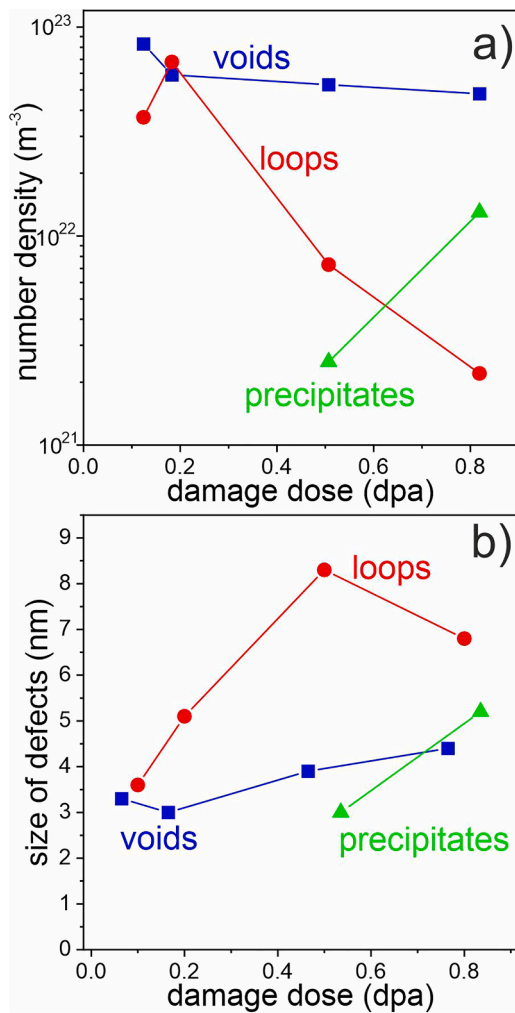


**Fig. 3.** The average size (a) and number density (b) of voids, dislocation loops and precipitates as function of damage doses.

were taken across voids and loops. The examples are shown in Fig. 6(e<sub>1</sub>-e<sub>3</sub>). Profiles (e<sub>1</sub>) and (e<sub>3</sub>) were taken transversely to voids marked by arrows (1 and 3). The intensity profiles show the typical reduction in *Re* intensity at the void position and the formation of elongated, Os-rich

regions adjacent to the void on one side. In the case of the void (3) of 3.0 nm size, these reduction of *Re* intensity is not as pronounced as in the case of the void (1) 6.0 nm size. The particles marked (2) in could serve as examples of the clouds that are not associated with a void. The *Re* profile does not show a typical for the voids a reduction of intensity in the middle (Fig. 6e<sub>2</sub>). The Os rich core of elongated shape is also located in the middle of the *Re* cloud. The Os rich cores show a crystallinity in the few cases. It can be assumed that the cores are precursors for the formation of precipitates on the later irradiation stages. In the few cases where crystallinity was detected, an exact identification of a crystalline phase appears to be not possible, as only one atomic plane of 0.23 nm could be identified. However, the atomic spacing of 0.23 nm corresponds to the [111] atomic plane of the  $\chi$ -WRe<sub>2</sub> phase, so it can only be considered as an indication of its formation.

### 3.3. *Re* and *Os* segregation on dislocations and grain boundaries

*Re* and *Os* segregate not only at the radiation-induced defects, but also at line dislocations and grain boundaries (Figs. 2, 4, 7, 8). It was found that segregation occurs even at the lowest damage doses, where the *Re* content is about 0.4 % (Fig. 2). At higher damage doses and thus higher *Re* and *Os* content, segregation was also observed at line dislocations (Figs. 2c, 7). Fig. 7 shows the *Re* (a) and *Os* (b) elemental maps of an area with grain boundaries and line dislocations. The *Re* and *Os* profiles shown in sections (c) and (d) reflect the intensity distribution over a grain boundary in the area marked (1) and the line dislocation marked (2). *Re* is enriched over a ~6.5 nm wide layer around a grain boundary, while *Os* is localized in a 3.5 nm layer on the grain boundary. The *Re* concentration inside the layer was measured to ~4 %, while *Os* accounts only 1.0 %. A similar distribution was also found around a line dislocation, where width of the *Re*-rich region around a line dislocation is approximately the same as for a grain boundary. The very narrow *Os* enriched area is show a local *Os* content of 0.5 %, which is considered to be within the detection range.

Also detailed analysis show that *Re* and *Os* segregation on the sub-grain boundaries takes place but these elements does not form a continuous layer and segregate on boundary dislocations. Fig. 8 shows analytical investigations of an inclined sub-grain boundary that is visible as a dislocation network in an image obtained with *g*[110] (a). The *Re* and *Os* elemental maps demonstrate that *Re* segregate preferably on the grain dislocations (b), whereas *Os* segregation is not clearly detected. The *Re* intensity profile shows that a dislocation network has a periodicity of about 25 nm (d).

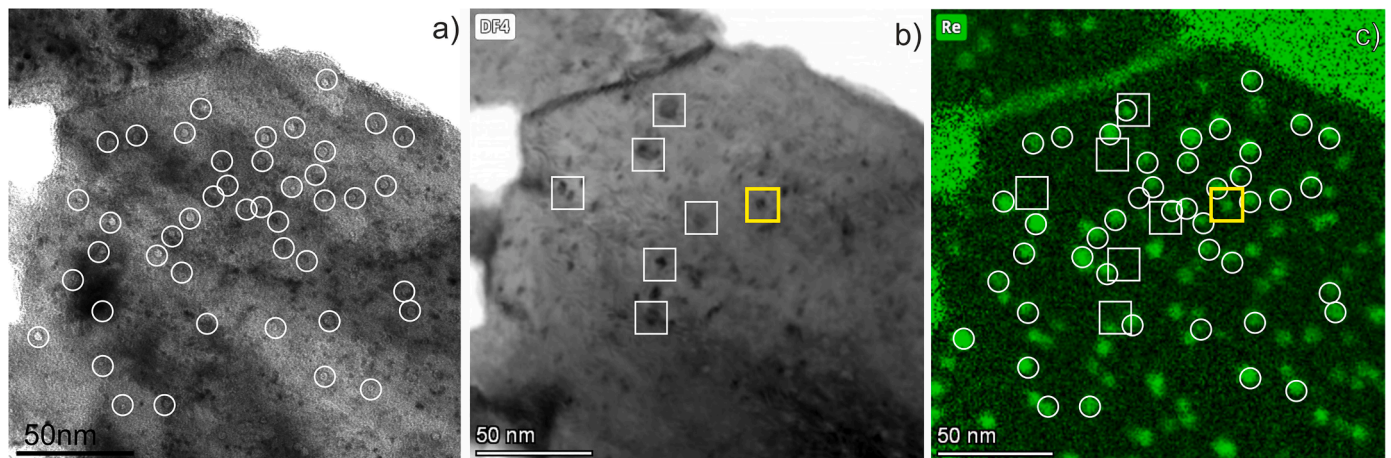


**Fig. 4.** Analytical study of the *Re*-segregation in material irradiated to 0.2 dpa. Part (a) shows a BF image, (b) is a DF image with inverted contrast and (c) the *Re* distribution in the examined region. The voids and their *Re*-clouds surrounding them are indicated by circles in (a) and (c), while the position of the loops is shown by squares in (b) and (c).

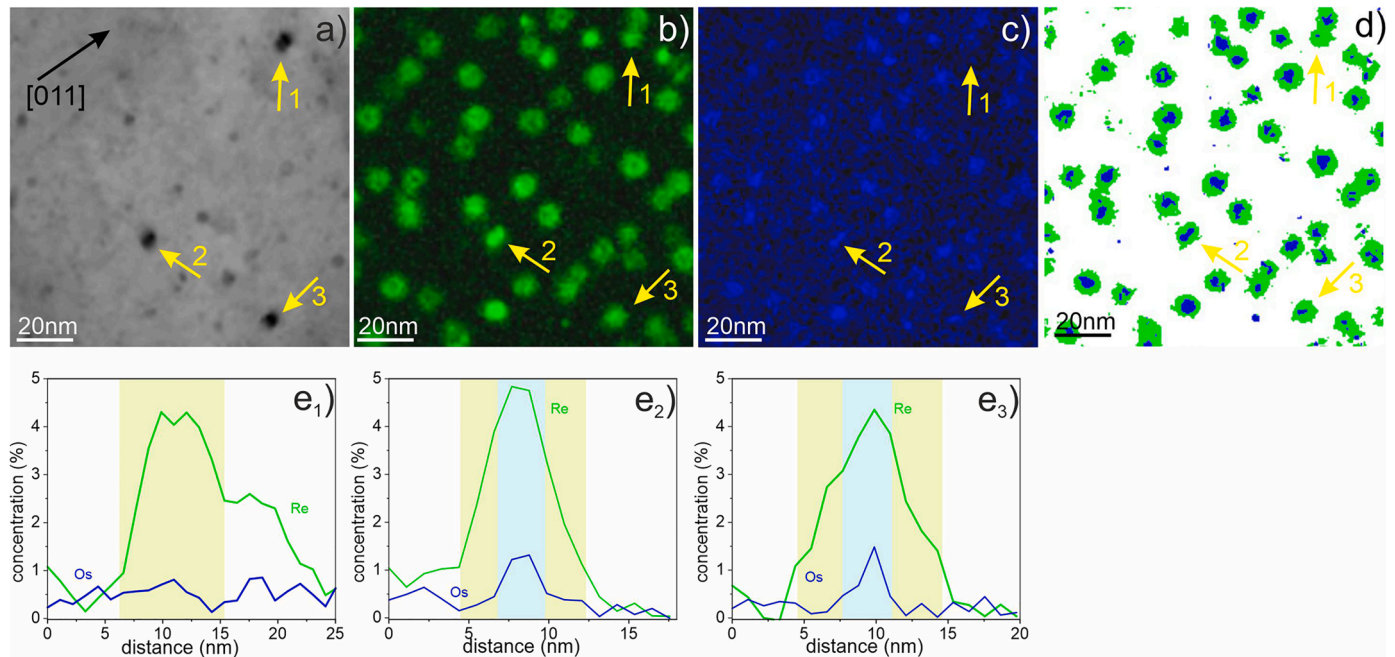


**Fig. 5.** Investigation of *Re*- and *Os*-segregation at dislocation loops in the sample irradiated to 0.5 dpa. Part (a) shows a DF image taken with inverted contrast of the investigated area. Parts (b) and (c) show the *Re* and *Os* distributions, respectively. The part (d) demonstrate overlap of measured *Re* (green) and in-core *Os* (blue) distribution. The *Os* and *Re* intensity profiles across numbered defects are show in parts (e<sub>1</sub>), (e<sub>2</sub>) and (e<sub>3</sub>).

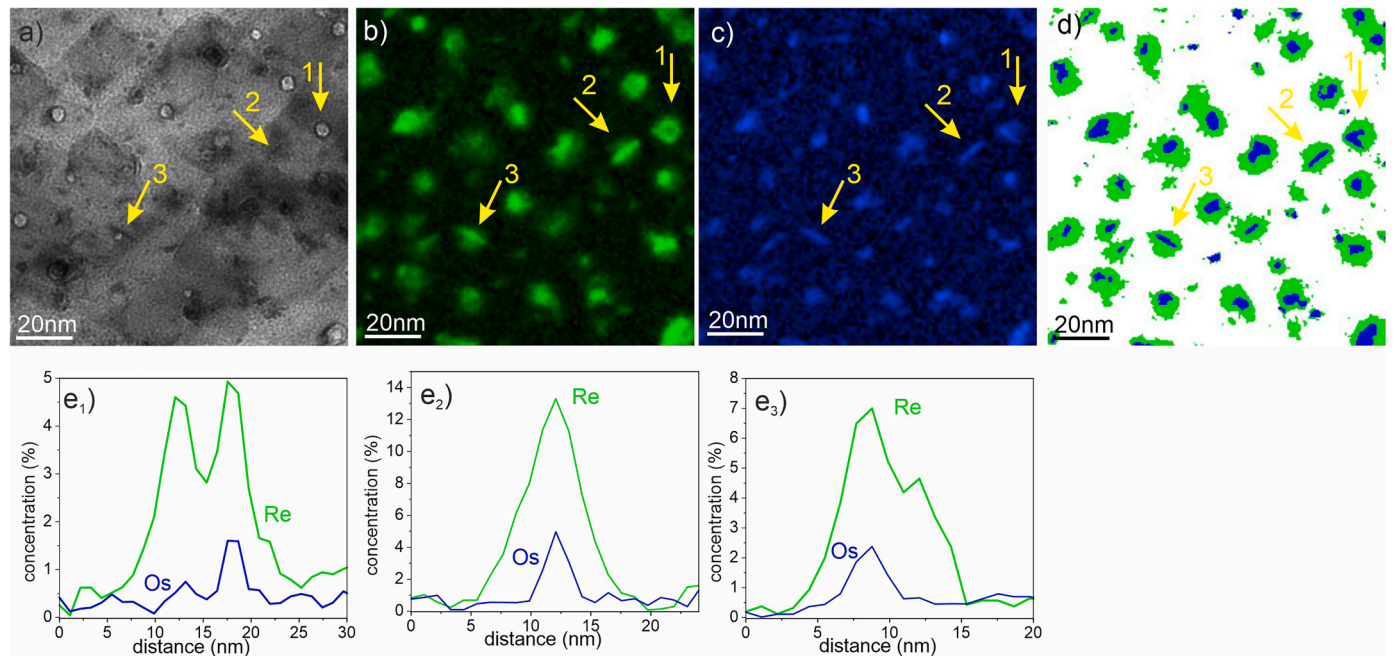


**Fig. 6.** Investigation of *Re*- and *Os*-segregation at voids and dislocation loops in the sample irradiated to 0.8 dpa. Part (a) shows a BF image of the investigated area. Parts (b) and (c) show the *Re* and *Os* distributions, respectively. The part (d) demonstrate overlap of measured *Re* (green) and *Os* (blue) distribution. The *Os* and *Re* intensity profiles across numbered defects are show in parts (e<sub>1</sub>), (e<sub>2</sub>) and (e<sub>3</sub>), respectively.

## 4. Discussion

### 4.1. Influence of *Re* and *Os* accumulation on the defect formation

Studies on neutron-irradiated W over the last two decades have shown that defect formation is closely related to the content of transmutation-induced *Re* and *Os*. Tanno et al. [9] demonstrated that the microstructure and mechanical properties of W and W-*Re* alloys are

strongly influenced by the *Re* content. In the study published by Hasegawa et al. [7], it was shown that defects formation in pure W strongly depends on the transmutation rate and consequently on the final *Re* content. W irradiation in HFIR reactor (Oak Ridge national Laboratory, USA) up to 2.5 dpa leads to the formation of 15 % transmutation elements, and consequently to an increased precipitates formation [12]. On the other side, the formation of the *Re* containing precipitates in pure W was not reported in pure W irradiated in Japanese reactor JOYO (fast

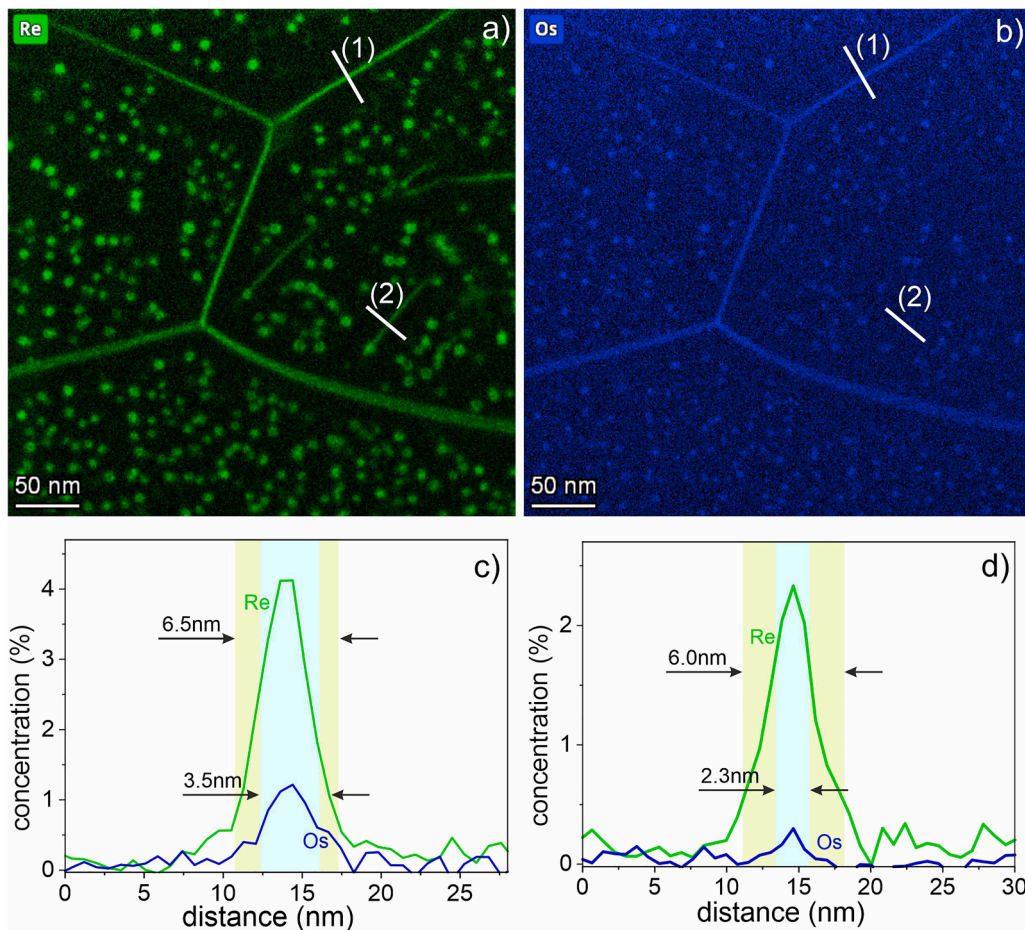


**Fig. 7.** Analytical study of the *Re* and *Os* segregation on structural defects. The element maps shown in (a) and (b) illustrate the distribution of *Re* and *Os*, respectively. The diagrams in parts (c) and (d) display the *Re* and *Os* intensity line scan across a grain boundary (1) and a line dislocation (2).

reactor, Japan Atomic Energy Agency, Japan) [8,12,20]. The reason for these differences are the transmutation rates in HIFR and JOYO reactors, which differ by a factor of 8–10. The presence of precipitates in W irradiated in BR2 (Belgian Reactor 2, Mol, Belgium) reactor was clearly observed after irradiation to  $\sim 1$  dpa and higher, when the *Re*/*Os* content reached  $\sim 2.5$  %. As has been shown, the different content of transmutation elements influences not only the precipitates formation, but also the formation of voids and especially dislocation loops.

Considering the damage - temperature defect formation diagram proposed by Hasegawa [7] and later modified by Marian [13], it can be concluded that at  $T_{irr} > 450$  °C both dislocation loops and voids are formed at the lowest damage doses. The dislocation loops disappear in a damage range between 0.7 dpa and 1 dpa with the formation of  $\chi$ -phase precipitates. It is therefore reasonable to assume that the disappearance of loops and the formation of precipitates are interrelated processes. Presumably, this process was initiated by a segregation of transmutation products in loops and voids, as experimentally demonstrated by EDX mapping and APT [6,12,21]. This *Re*- and *Os* segregation can be considered as a kind of precursor to the formation of precipitates. It should be mentioned that *Re*/*Os* rich "clouds" around defects are not visible in TEM images obtained by BF- or DF-TEM imaging and its visualization required the use of high sensitivity EDX or APT analyses. *Re*/*Os* segregation does not induce local stresses in a lattice that could be visualized by diffraction contrasts in TEM. Therefore, the formation of precipitates is visible only when *Re*/*Os*-rich particles with a crystallographic structure are formed, that is different from the surrounding matrix. This however occurs only at higher irradiation stages, where needle-like  $\chi$ -phase precipitates were formed [4,22].

Based on the analytical results shown in Figs. 3–8, a sequence of *Re*- and *Os* segregation and subsequent precipitate formation was drawn in the Fig. 9. The individual steps in the sequence can be briefly described as follows:

- The voids and dislocation loops are formed in W under neutron irradiation at damage doses below 0.1 dpa when the content of transmutation element is negligible (a). At 0.1 dpa damage, local *Re* content around the voids reaches few percent and can be detected by EDX method (b) and at 0.2 dpa *Re* segregation could be additionally measured at the dislocation loops with size larger than 10 nm (c).
- At a damage dose of 0.5 dpa, the *Os* content in *Re* reaches a detectable level. *Os*-rich regions form within *Re* clouds around voids and on dislocation loops (d). In the process, the number density of the loops is reduced by a factor 10 compared to the material with 0.2 dpa damage.
- Further accumulation of transmutation products (in this case at 0.8 dpa) leads to the formation of nanocrystalline  $\chi$ -phase precipitates on both loops and voids (e). As a result, a dislocation loops disappears - or it is no longer visible as a loop, whereas voids are visible with attached on them precipitates even at high damage doses.

The TEM analysis shows that the void and loop structures change significantly in the W irradiated at 0.5 dpa, where the total enrichment of the transmutation elements is 1.2 % and more. In the process, the density of the loops decreases significantly by one order of magnitude

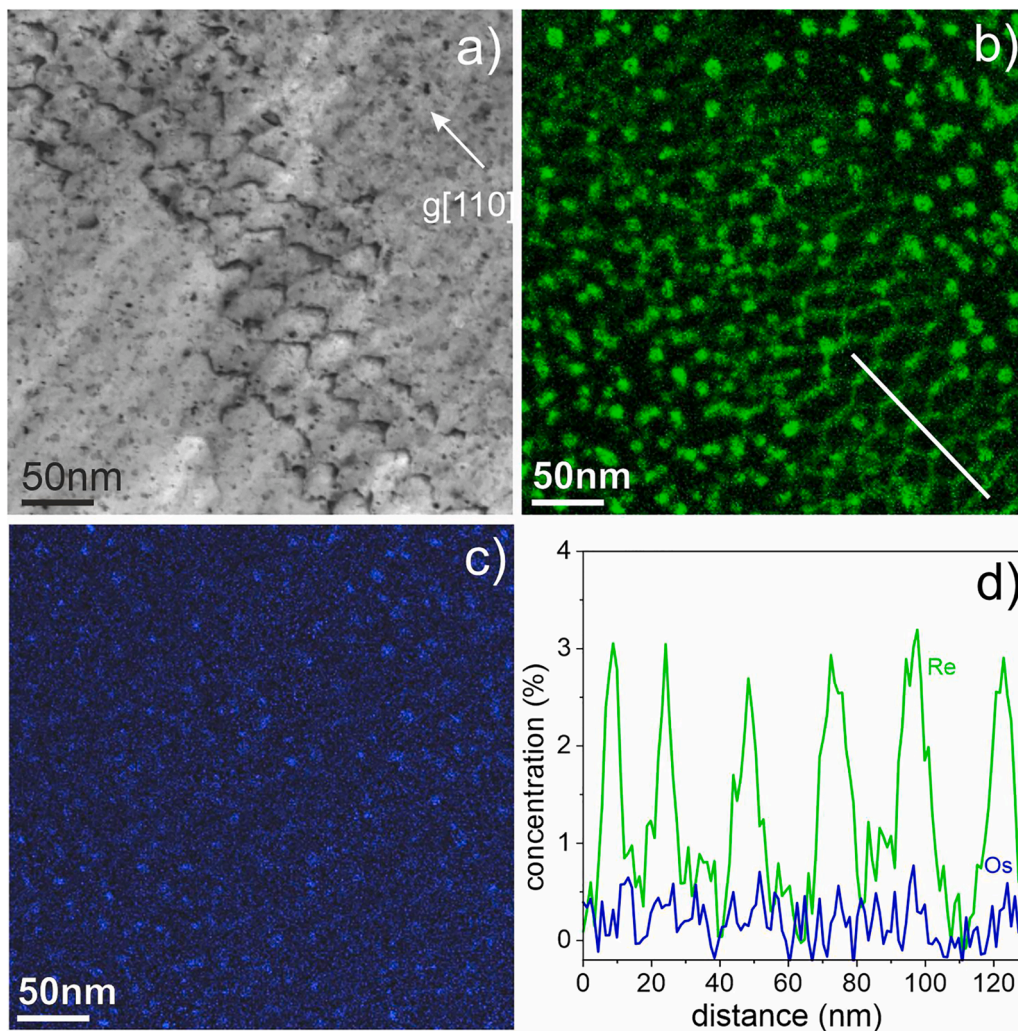


**Fig. 8.** Analytical study of the *Re* and *Os* segregation on a two-dimensional dislocation network, Part (a) show a dark field [110] *g*-image with inverted contrast of investigated area. The element maps shown in (b) and (c) illustrate the distribution of *Re* and *Os* respectively. The diagram in parts (d) display the *Re* and *Os* intensity line scan across a line marked in the part (b).

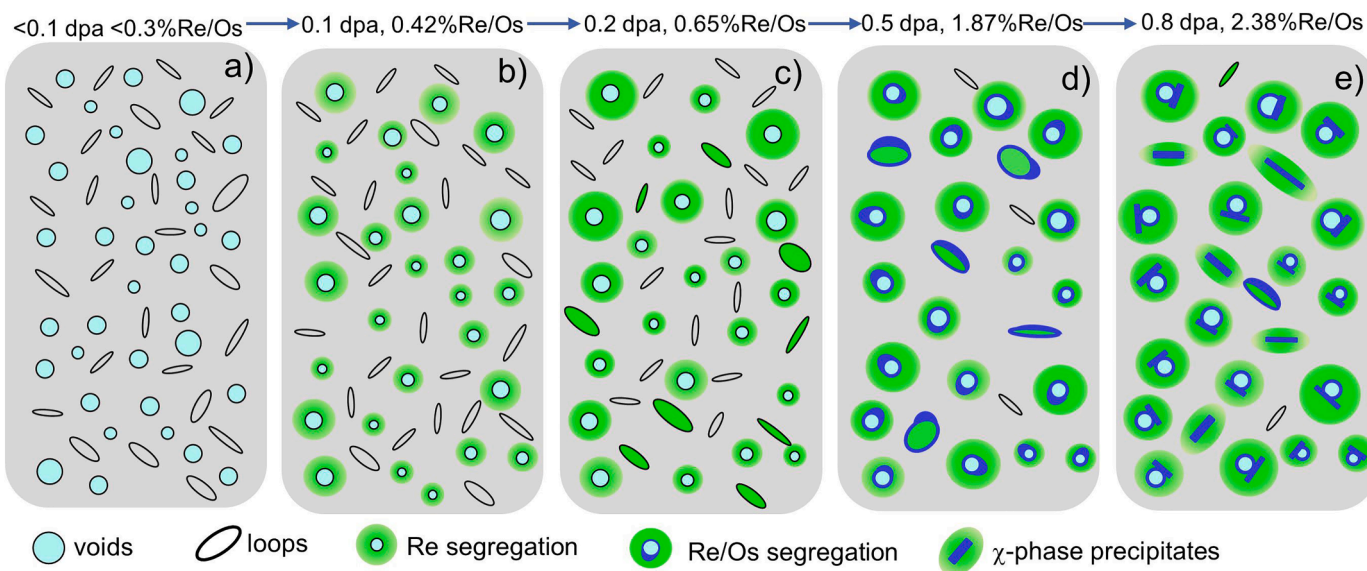


**Fig. 9.** Schematic sequence demonstrating the defect formation stages in W considering the *Re* and *Os* segregation on defects. See text for more details.

and the first formation of precipitates was observed (Fig. 3). According to the modified Hasegawa diagram shown in Refs. [7,13], one might expect that at 1 dpa a process begins that finally leads to the disappearance of the loops and the formation of precipitates. Our results provide a detailed view of microstructural evolution of W in this damage range and may help to understand this process.

- (a) (Fig. 9a) In the present study, well-developed voids and loop structure were observed at 0.1 dpa (Fig. 1). The void structure does not change significantly upon further irradiation up to 0.8 dpa, where their size increases from 3 to 4.5 nm, while the number density decreases by 25 % (Fig. 3). It can be concluded that saturation of voids and loop structures is complete at damage doses below 0.1 dpa, so that further damage doses would cause only minor changes. The results shown in a previous study confirm this supposition and show that voids and dislocation loops form in W at damage doses below 0.03 dpa [8]. This formation of voids and loops on the initial irradiation stages (below 0.1 dpa) is illustrated in Fig. 9a.
- (b) (Fig. 9b) Transmutation induced Re and Os were found to form spherical rich areas “clouds” around voids, dislocation loops and on the grain boundaries at ~1 dpa damage [6,10]. In the present work, it was found that Re segregation on voids and grain boundaries already takes place at 0.1 dpa with Re content of 0.2 at.% (Fig. 2a,a’). At 0.2 dpa, the Re content in the clouds around voids increases (circles in Fig. 4a,c). However the Re segregation on dislocation loops, that are marked by squares in Fig. 4a,c was detected only on few loops. This irregular segregation suggests that loops form continuously during irradiation and that loops formed at later stages of irradiation do not accumulate a detectable Re content.
- (c) (Fig. 9d) At 0.5 dpa, the number density of dislocation loops decreases by almost an order of magnitude and their average size increases remarkably. Re and Os were found to segregate on voids and dislocation loops. Since Os is formed by the transmutation of Re, it is preferentially generated within Re clouds on voids and loops, where it forms well-detectable Os-rich regions (Fig. 5). The implications of Re and Os segregation on the visibility of the loops are illustrated by the example of the 3 loops numbered in the images (Fig. 5). The loop (1) does not have a pronounced Os rich core, whereas both other loops, (2 and 3) show an Os rich region of about 2nm\*6 nm (Fig. 5d). The Re forms 8–10 nm clouds around the loop. Presumably Os preferably segregates on the dislocation of the loops, as shown in Ref. [10,21]. Os segregation on the loops was found to have an effect on the visibility of the loops in the TEM images, and presumably on the local stress created by the loops. Loop (1), which doesn’t show any Os segregation, is visible with the “coffee bean” contrast typical of a loop, whereas loops (2) and (3), which have pronounced Os segregation, do not have this contrast. It is well known that this contrast around dislocation loops or nanosized precipitates is caused by the local lattice stress in the adjacent areas. The disappearance of this contrast in the loops (2) and (3) indicates that the local stress is possibly reduced by Os accumulation. However, Os does not form a crystalline structure at this irradiation stage. High resolution TEM analysis does not show the formation crystalline precipitates. It can also be assumed that Re-rich clouds around dislocation loops dissolve when the loop disappears. This also suggests that a Re-rich cloud without a structural defect is not an attractive target for interstitials.
- (d) (Fig. 9c) The W microstructure show significant changes when the damage dose increases from 0.5 dpa to 0.8 dpa. Needle-shaped precipitates with high Os content were observed at almost all voids (voids (1) and (3) in Fig. 6). The Re and Os intensity profiles demonstrate that precipitates are attached to the voids (void (1) in Fig. 6)). In addition to the voids, a small number

of precipitates could have formed independently of the voids (arrow (2) in Fig. 6)). The Re and Os profiles of such precipitates show a clear similarity to the Re and Os segregation on dislocation loops as shown in Fig. 5, however, a loop is not visible even in this case. From the analytical study of W at lower damage doses, one can conclude that only two types of radiation induced defects - dislocation loops or voids - serve as segregation sites for transmutation-induced Re and Os. Consequently, all precipitates that did not form on voids originated from dislocation loops that disappeared when the precipitates formed. The further reduction of loop number density and increase that of precipitates at 0.8 dpa damage confirm this conclusion (Fig. 3).

The formation of the precipitates independent of the voids was also observed in W irradiated to 1.6 dpa in the HFR reactor (Petten) [6] and to ~1 dpa in the BR2 reactor [10]. It was also mentioned that the differentiation of dislocation loops from precipitates in TEM images is difficult and leads to a significant statistical error in their statistic. It is also possible that some loops with Re/Os segregation are both a dislocation loop and a precipitate. Nevertheless, a few loops that have a typical “coffee-bean” contrast were also found in this sample. These loops possibly did not accumulate Re and Os in sufficient quantity for transformation into precipitates.

This assumption can be confirmed by the analysis of W irradiated at 1100 °C to 1.05 dpa in the BR2 reactor (Fig. 10). The W irradiated at this irradiation conditions contains about 2.2 % Re and Os. The EDX analyses clearly show a Re-segregation at dislocation loops with a size of about 10–15 nm, which are visible in the DF image with “coffee bean” contrast (yellow arrows). These loops show a noticeable Re-rich cloud around them, but also a very weak Os-rich cores. The smaller dislocation loops with a size of ~5 nm do not show any detectable segregation of transmutation products. Presumably, the smaller loops formed on the later stages and following the Re-segregation around them is not sufficient to be identified. These results support the interpretation presented here for the differences in Re contents around dislocation loops. The detailed microstructural analysis of this sample is shown in ref. [10].

#### 4.2. Defect formation diagram in neutron irradiated W

A diagram that illustrates the formation of radiation-induced defects as a function of damage dose and temperature was first proposed by Hasegawa et al. [23] and further modified by Marian et al. [13] and Koyanagi et al. [8]. The diagrams show that dislocation loops and voids are formed at low damage doses and  $T_{irr} > 500$  °C. In the more recent Marian and Koyanagi diagrams was shown that in the damage range between 0.7 and 1.3 dpa dislocation loops disappear and the formation of precipitates was observed. It has also been suggested that these processes are associated with the accumulation of transmutation products. The diagram of Marian reflects defect formation in W irradiated in Japanese fast reactor JOYO with lower transmutation rate (~1.0 % Re/Os per dpa). The diagram of Koyanagi, however, includes preferentially the results on W irradiated in HFIR (Oak Ridge) with transmutation rates of ~8–9 % Re/Os per dpa. It can be concluded that pure W irradiated in these reactors with the same damage dose at the same temperature differs in the content of transmutation elements by a factor of 8. Accordingly, these are different materials that can exhibit a different microstructure after irradiation. For this reason, the proposed diagrams can only be used for the prediction of defects formation in W irradiated in the same reactor. Considering that defect formation depends largely on the content of transmutation products and less on the damage dose, we propose to modify this diagram in a way that the x-axis indicates the concentration of transmutation products and not the damage dose (Fig. 11). This would allow to predict a defects formation independently of the reactor type.

The second modification concerns the occurrence of defects (or their presence in the final state) under certain conditions. The results shown

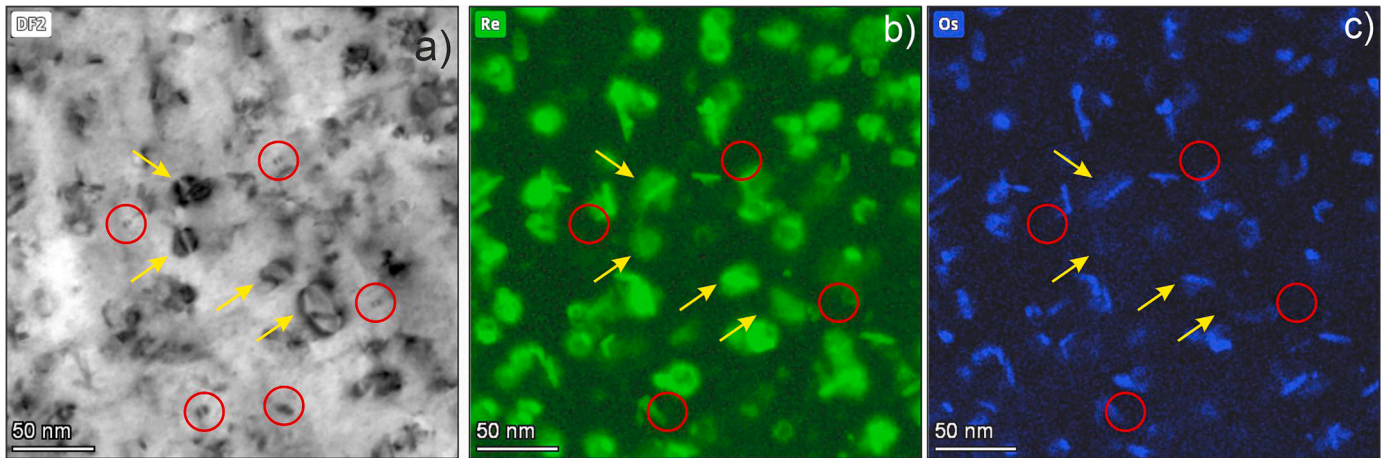


Fig. 10. Re and Os segregation on dislocation loops in W irradiated at 1100 °C to 1.05 dpa. The yellow arrows indicate large >15 nm loops in DF image with reverse contrast (a) and their positions in Re (b) and Os (c) maps, whereas red circles show the positions of dislocation loops with a size of ~5 nm [10].

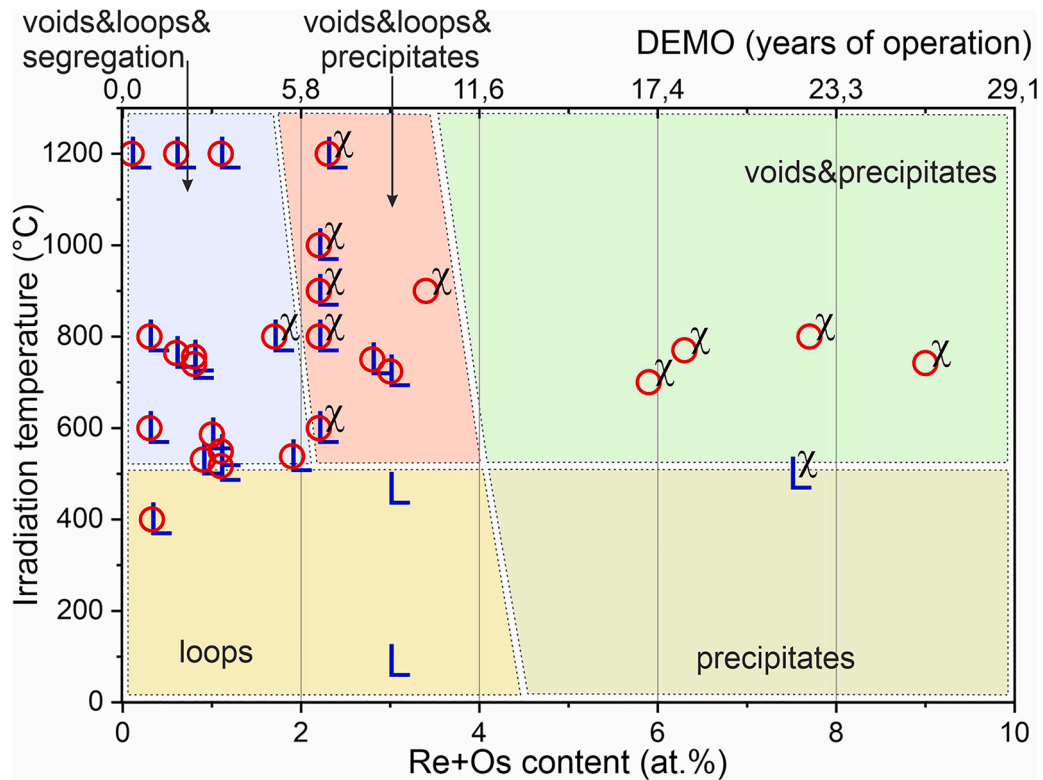


Fig. 11. The modified defect formation diagram in neutron irradiated W that shows conditions for formation of voids (O), loops (L) and precipitates ( $\chi$ ) depending on the Re and Os content. The data were taken from Refs. [7,10,13].

in Figs. 1 and 2 demonstrate that the void population has been formed at the damage doses below 0.1 dpa, where the influence of transmutation products is negligible. Possibly the irradiation temperature and dose rate play a decisive role in the evolution of defects during initial irradiation stages. The segregation of transmutation induced Re on voids could be detected at 0.1 dpa (0.42 % Re/Os content). Despite the number density of the loops is in the same order of magnitude as the voids, the segregation on the loops is too low to be detected using EDX. A segregation on few loops could be detected in material irradiated to 0.2 dpa, when Re and Os content increases to 0.6 %. It can be suggested that loops formation in W is a dynamic process that includes the constant formation and dissolution of the loops. The larger loops that may have formed in the initial phase accumulated a higher Re content. The number density

of loops reduced significantly in W irradiated at 0.5 dpa (1.87 % Re/Os content), so that presumably higher Re content prevents the formation of new loops. The first formation of precipitates was detected at 0.5 dpa (1.87 % Re/Os content) and their number increases significantly in the W irradiated to 0.8 dpa (2.38 % Re/Os content). Despite the number density of the loops significantly reduces. To summarize, there is a range of Re/O contents between 1.8 % and ~4 % in which the presence of voids, loops and precipitates could be observed (Fig. 11).

A modelling study carried out on the Fe-Ni system shows that the specific partitioning of atoms and point defects generated by neutron irradiation can shift the phase boundaries indicated in the equilibrium phase diagrams [24]. It may cause the precipitation of it may cause the precipitation of chemical phases which do not even exist in equilibrium

phase diagrams. In the neutron-irradiated W, precipitates formation starts at  $\sim 2\%$  Re/Os concentration, that is below the 26% Re specified as the lower range for the formation of  $\chi$ -phase in the Re-W phase diagram.

As the precipitates form, the density of the dislocation loops decreases significantly (Fig. 3). It can be assumed this process can be influenced by the void number density. At a high number density of voids, there are many sites for Re and Os segregation, and thus the local concentration around voids or loops remains below a level required for the precipitate formation. At low void density, the formation of precipitates could start at lower Re/Os content as it reaches a higher local concentration in the clouds around the voids. However, there are not sufficient experimental results showing what processes occur at low temperature and high content of transmutation elements.

It can be assumed that the precipitates, which form independently of the voids, have their origin in dislocation loops. The precipitates found independent of the voids could presumably have been formed at the dislocation loops that disappeared at the irradiation stage at which the sample was analyzed. The formation of nano-sized  $\chi$ -phase precipitates separately from the voids was reported by Klimenkov et al. [6]. It was found that in single crystal W irradiated in HFR to 1.6 dpa, only about 50% precipitates are formed around the voids and the other half are formed separately of them. The presence of nano-sized precipitates which formation does not connect to the voids was also reported in ref. [10].

Our results also allow prediction of microstructural evolution when pure tungsten is exposed to the DEMO fusion first wall conditions (upper scale in Fig. 11). The data concerning the production of transmutation elements as a function of operating time were taken from the ref. [25]. The diagram shows that the disappearance of the loops and the formation of precipitates starts after about 5 years and is completed after about 10 years of DEMO operation. After 10 years of operation, it is expected that only voids and precipitates remain in the W.

#### 4.3. Segregation on grain boundaries and line dislocations

Previous works have shown that Re and Os segregate not only on radiation-induced defects, but also on the structural defects that were present in W before irradiation, e.g., line dislocations and grain boundaries [6,10]. EDX analyses reported in Ref. [10] has also shown that Re often does not form a continuous layer on grain boundaries, but is deposited on grain boundary dislocations. The allocation of much sensitive APT method has confirmed these results [21]. In that case elemental maps show that Re forms a discrete spots with 15 nm-25 nm periodicity on a grain boundary and not a homogeneous layer. When the dislocation lines are oriented perpendicular to the sample surface (or parallel to the electron beam), their projections are visible as points and not as lines in the TEM images. In most cases, however, the dislocation network, and thus the grain boundary, are visible as a continuous layer when the dislocations overlap in the images to each other.

The results presented here show that transmutation induced Re and Os segregate at grain boundaries in a detect even at a very low damage dose, where the Re content is less than 0.2 at.% (Fig. 2a,b). At 0.5 dpa and above, Re at grain boundaries is present in association with Os. The intensity line scan demonstrates that Re is enriched in an area of 6.5 nm around grain boundary, whereas Os is segregated inside 3.5 nm this area (Fig. 7a,c). A similar segregation behavior was observed considering the analytical study of dislocation lines (Fig. 7b,d).

In Fig. 8, an inclined sub-grain boundary is shown that was formed by a dislocation network. The example clearly shows that Re-segregation occurs at grain boundary dislocations, while the Os signal is too weak to be detectable. Analysis of the previously published results suggests that formation of precipitates on grain boundaries take place only at Re and Os content higher than 10% [12]. However, the precipitates at the boundaries are larger than those formed on radiation-induced defects. Probably this is due to the Re- and Os-diffusion along the boundary.

## 5. Conclusions

This study presents the results of extensive microstructural analyses of W that was neutron irradiated at 1200 °C to a damage doses of 0.1, 0.2, 0.5 and 0.8 dpa. The study includes the identification and analysis of radiation induced defects such as voids and dislocation loops, as well as analytical study of Re and Os segregation at different damage doses. The results of the study can be summarized as follows:

- Voids and dislocation loops were detected at all damage doses. While the size and number density of voids do not change significantly with damage, the number density of dislocation loops decreases significantly at 0.5 dpa and higher damage.
- Re segregation at voids and grain boundaries could be detected at the lowest damage dose of 0.1 dpa, while Re and Os segregation at dislocation loops was detected at 0.5 dpa.
- It was shown that Re segregation at dislocation loops and especially accumulation of Os finally leads to the formation of  $\chi$ -phase precipitates on dislocation loops. Dislocation loops disappear during this transformation.
- A defect formation sequence was drawn that takes into account not only the evolution of loops and voids, but also the Re and Os segregation starting from the low damage (and herewith low Re/Os content) and their effects on defect formation.
- Summarizing these results, it can be stated that the Re and Os content plays a more important role in defect evolution than the damage dose. Consequently, a modification of the defect formation diagram of Hasegawa [7,13] is proposed, so that the diagram shows the defect formation depending on the Re and Os content.
- The new diagram also allows the prediction of the microstructural evolution for the W irradiated under fusion conditions.

#### CRediT authorship contribution statement

**M. Klimenkov:** Conceptualization, Data curation, Writing – original draft, Writing – review & editing, Investigation. **U. Jäntschi:** Data curation, Investigation. **M. Rieth:** Conceptualization, Resources, Supervision. **H.C. Schneider:** Data curation, Methodology. **D. Terentyev:** Conceptualization, Data curation, Validation. **W. Van Renterghem:** Data curation, Investigation.

#### Declaration of competing interest

The authors declare that they have no known competing financial interests or personal relationships that could have appeared to influence the work reported in this paper.

#### Data availability

Data will be made available on request.

#### Acknowledgments

This work has been carried out within the framework of the EUROfusion Consortium, funded by the European Union via the Euratom Research and Training Programme (Grant Agreement No 101052200 — EUROfusion). Views and opinions expressed are however those of the author(s) only and do not necessarily reflect those of the European Union or the European Commission. Neither the European Union nor the European Commission can be held responsible for them.

## References

- [1] H. Bolt, V. Barabash, W. Krauss, J. Linke, R. Neu, S. Suzuki, N. Yoshida, A.U. Team, Materials for the plasma-facing components of fusion reactors, *J. Nucl. Mater.* 329–333 (2004) 66–73, <https://doi.org/10.1016/j.jnucmat.2004.04.005>.
- [2] M. Rieth, R. Doerner, A. Hasegawa, Y. Ueda, M. Wirtz, Behavior of tungsten under irradiation and plasma interaction, *J. Nucl. Mater.* 519 (2019) 334–368, <https://doi.org/10.1016/j.jnucmat.2019.03.035>.
- [3] M.J. Lloyd, R.G. Abernethy, M.R. Gilbert, I. Griffiths, P.A. Bagot, D. Nguyen-Manh, M.P. Moody, D.E. Armstrong, Decoration of voids with rhenium and osmium transmutation products in neutron irradiated single crystal tungsten, *Scr. Mater.* 173 (2019) 96–100, <https://doi.org/10.1016/j.scriptamat.2019.07.036>.
- [4] A. Hasegawa, M. Fukuda, K. Yabuuchi, S. Nogami, Neutron irradiation effects on the microstructural development of tungsten and tungsten alloys, *J. Nucl. Mater.* 471 (2016) 175–183, <https://doi.org/10.1016/j.jnucmat.2015.10.047>.
- [5] T. Hwang, A. Hasegawa, K. Tomura, N. Ebisawa, T. Toyama, Y. Nagai, M. Fukuda, T. Miyazawa, T. Tanaka, S. Nogami, Effect of neutron irradiation on rhenium cluster formation in tungsten and tungsten-rhenium alloys, *J. Nucl. Mater.* 507 (2018) 78–86, <https://doi.org/10.1016/j.jnucmat.2018.04.031>.
- [6] M. Klimenkov, U. Jäntschi, M. Rieth, H.C. Schneider, D. Armstrong, J. Gibson, S. G. Roberts, Effect of neutron irradiation on the microstructure of tungsten, *Nucl. Mater. Energy* 9 (2016) 480–483, <https://doi.org/10.1016/j.nme.2016.09.010>.
- [7] A. Hasegawa, M. Fukuda, S. Nogami, K. Yabuuchi, Neutron irradiation effects on tungsten materials, *Fusion Eng. Des.* 89 (2014) 1568–1572, <https://doi.org/10.1016/j.fusengdes.2014.04.035>.
- [8] T. Koyanagi, N.K. Kumar, T. Hwang, L.M. Garrison, X. Hu, L.L. Snead, Y. Katoh, Microstructural evolution of pure tungsten neutron irradiated with a mixed energy spectrum, *J. Nucl. Mater.* 490 (2017) 66–74, <https://doi.org/10.1016/j.jnucmat.2017.04.010>.
- [9] T. Tanno, M. Fukuda, S. Nogami, A. Hasegawa, Microstructure development in neutron irradiated tungsten alloys, *Mater. Trans.* 52 (2011) 1447–1451, <https://doi.org/10.2320/matertrans.MBW201025>.
- [10] M. Klimenkov, M. Dürrschnabel, U. Jäntschi, P. Lied, M. Rieth, H.C. Schneider, D. Terentyev, W. van Renterghem, Microstructural analysis of W irradiated at different temperatures, *J. Nucl. Mater.* 572 (2022) 154018, <https://doi.org/10.1016/j.jnucmat.2022.154018>.
- [11] W. van Renterghem, G. Bonny, D. Terentyev, TEM investigation of neutron irradiated and post irradiation annealed tungsten materials, *Fusion Eng. Des.* 180 (2022) 113170, <https://doi.org/10.1016/j.fusengdes.2022.113170>.
- [12] X. Hu, C.M. Parish, K. Wang, T. Koyanagi, B.P. Eftink, Y. Katoh, Transmutation-induced precipitation in tungsten irradiated with a mixed energy neutron spectrum, *Acta Mater.* 165 (2019) 51–61, <https://doi.org/10.1016/j.actamat.2018.11.032>.
- [13] J. Marian, C.S. Becquart, C. Domain, S.L. Dudarev, M.R. Gilbert, R.J. Kurtz, D. R. Mason, K. Nordlund, A.E. Sand, L.L. Snead, T. Suzudo, B.D. Wirth, Recent advances in modeling and simulation of the exposure and response of tungsten to fusion energy conditions, *Nucl. Fusion* 57 (2017) 92008, <https://doi.org/10.1088/1741-4326/aa5e8d>.
- [14] X. Hu, Recent progress in experimental investigation of neutron irradiation response of tungsten, *J. Nucl. Mater.* 568 (2022) 153856, <https://doi.org/10.1016/j.jnucmat.2022.153856>.
- [15] A. Dubinko, D. Terentyev, C. Yin, W. van Renterghem, B. Rossaert, M. Rieth, E. Zhurkin, A. Zinovev, C.C. Chang, S. van Dyck, G. Bonny, Microstructure and hardening induced by neutron irradiation in single crystal, ITER specification and cold rolled tungsten, *Int. J. Refract. Met. Hard Mater.* 98 (2021) 105522, <https://doi.org/10.1016/j.jrmhm.2021.105522>.
- [16] D.B. Pelowitz, J.W. Durkee, J.S. Elson, M.L. Fensin, J.S. Hendricks, M.R. James, R. C. Johns, G.W. Mc Kinney, S.G. Mashnik, L.S. Waters, T.A. Wilcox, J.M. Verbeke, MCNPX 2.7.0 extensions, 2011.
- [17] S. Hasanzadeh, R. Schäublin, B. Décamps, V. Rousson, E. Autissier, M.F. Barthe, C. Hébert, Three-dimensional scanning transmission electron microscopy of dislocation loops in tungsten, *Micron* (Oxford, England 1993) 113 (2018) 24–33, <https://doi.org/10.1016/j.micron.2018.05.010>.
- [18] C.T. Rueden, J. Schindelin, M.C. Hiner, B.E. DeZonia, A.E. Walter, E.T. Arena, K. W. Eliceiri, ImageJ2: imageJ for the next generation of scientific image data, *BMC Bioinform.* 18 (2017) 529, <https://doi.org/10.1186/s12859-017-1934-z>.
- [19] P. Xiu, H. Bei, Y. Zhang, L. Wang, K.G. Field, STEM characterization of dislocation loops in irradiated FCC alloys, *J. Nucl. Mater.* 544 (2021) 152658, <https://doi.org/10.1016/j.jnucmat.2020.152658>.
- [20] X. Hu, T. Koyanagi, M. Fukuda, N.K. Kumar, L.L. Snead, B.D. Wirth, Y. Katoh, Irradiation hardening of pure tungsten exposed to neutron irradiation, *J. Nucl. Mater.* 480 (2016) 235–243, <https://doi.org/10.1016/j.jnucmat.2016.08.024>.
- [21] M.J. Lloyd, A.J. London, J.C. Haley, M.R. Gilbert, C.S. Becquart, C. Domain, E. Martinez, M.P. Moody, P. Bagot, D. Nguyen-Manh, D. Armstrong, Interaction of transmutation products with precipitates, dislocations and grain boundaries in neutron irradiated W, *Materialia* (Oxf) 22 (2022) 101370, <https://doi.org/10.1016/j.mtla.2022.101370>.
- [22] M. Fukuda, K. Yabuuchi, S. Nogami, A. Hasegawa, T. Tanaka, Microstructural development of tungsten and tungsten–rhenium alloys due to neutron irradiation in HFIR, *J. Nucl. Mater.* 455 (2014) 460–463, <https://doi.org/10.1016/j.jnucmat.2014.08.002>.
- [23] A. Hasegawa, M. Fukuda, T. Tanno, S. Nogami, Neutron irradiation behavior of Tungsten, *Mater. Trans.* 54 (2013) 466–471, <https://doi.org/10.2320/matertrans.MG201208>.
- [24] M. Nastar, L.T. Belkacemi, E. Meslin, M. Loyer-Prost, Thermodynamic model for lattice point defect-mediated semi-coherent precipitation in alloys, *Commun. Mater.* 2 (2021), <https://doi.org/10.1038/s43246-021-00136-z>.
- [25] Y. Qian, M.R. Gilbert, L. Dezerald, D. Cereceda, Using first-principles calculations to predict the mechanical properties of transmuted tungsten under first wall fusion power-plant conditions, *J. Phys.* 33 (2021), <https://doi.org/10.1088/1361-648X/ac08b8>. Condensed matter an Institute of Physics journal.